A coupled ES-FEM and FM-BEM for structural acoustic problems

F. Wu[a),b)], G.R. Liu[b)], G.Y. Li[c)], Y.J. Liu[d)] and Z.C. He[e)]

(Received: 8 December 2013; Revised: 7 July 2014; Accepted: 9 July 2014)

In this paper, a coupled numerical method of the edge-based smoothed finite element (ES-FEM) with the fast multipole BEM (FM-BEM) is proposed to analyze structural acoustic problems. The vibrating structure is modeled using the so-called ES-FEM-DSG3 method, where the 3-node linear triangle plate elements based on the Reissner–Mindlin plate theory with the discrete shear gap (DSG) technique for overcoming the shear locking are applied. The edge-based gradient smoothing operations are applied to "soften" the "overly-stiff" behavior in the standard FEM, which significantly reduces the inherent numerical dispersion error. The normal velocities on the surface of the structure are imposed as boundary conditions for the acoustic domain which is modeled using the FM-BEM for both the interior and exterior acoustic domains. Comparing with the conventional BEM, the matrix vector multiplication and the memory requirement in the FM-BEM are reduced dramatically. The coupled ES-FEM/FM-BEM method takes the advantages of both ES-FEM and FM-BEM, which can avoid drawbacks of the "overly-stiff" behavior in FEM and computational inefficiency in the conventional BEM. Two numerical examples are presented to verify and demonstrate the effectiveness of the combined method: one academic problem for studying in detail the accuracy and efficiency of the present method, and one application to a practical vehicle noise simulation. © *2014 Institute of Noise Control Engineering.*

Primary subject classification: 75.3; Secondary subject classification: 75.5

1 INTRODUCTION

Noises generated by a vibrating thin structure can be commonly found in numerous engineering systems, such as aircrafts, sea vessels and the land vehicles. These acoustic problems are closely associated to fluid–structure interactions and are of increasing concern when designing passenger transportation systems. Many researchers have done great work to solve this kind of problems. The widely used methods are the standard finite element method (FEM) and/or the boundary element method (BEM)[1–3]. It is, however, widely realized that substantial improvements are needed to address the accuracy, efficiency and robustness of these methods for coupled structural acoustic problems.

FEM is extensively preferred to model the structure part of structural acoustic problems, where lower-order Reissner–Mindlin plate element is often chosen due to its efficiency and simplicity[4–6]. However, this method is well-known to have two inherent drawbacks. Firstly, the Reissner–Mindlin plate elements often suffer from the so-called "shear locking" problem in the thin plate case, which is resulted from the incorrect transverse shear strains under the pure bending condition[7]. The other one is the "overly-stiff" property of FEM in the numerical solution, which leads to a significant loss of accuracy[8]. In order to eliminate "shear locking" phenomenon, many numerical techniques and effective improvement of formulations have been proposed, such as the selective reduced integration scheme[9–11], free formulation method[12], and mixed formulation/hybrid elements[13,14]. Unfortunately, all these methods have some drawbacks like instability due to rank deficiency, inaccuracy and complex formulation. Then many new numerical techniques were developed to

a) State Key Lab of Advanced Technology for Vehicle Body Design and Manufacture, Hunan University, Changsha, 410082, CHINA; email: wufeifrank@gmail.com.
b) School of Aerospace Systems, University of Cincinnati 2851 Woodside Dr, Cincinnati, OH 45221, USA.
c) State Key Lab of Advanced Technology for Vehicle Body Design and Manufacture, Hunan University, Changsha, 410082, CHINA; email: gyli@hnu.cn (Corresponding author).
d) Mechanical Engineering, University of Cincinnati, 598 Rhodes, Cincinnati, OH 45221, USA.
e) State Key Lab of Advanced Technology for Vehicle Body Design and Manufacture, Hunan University, Changsha, 410082, CHINA.

further enhance the stability and accuracy of numerical solution. Such as enhanced assumed strain (EAS) methods[15,16] and assumed natural strain (ANS) methods[17,18]. Recently, the discrete shear gap (DSG) method, which works for elements of different orders and shapes, was developed for overcoming the "shear locking" phenomenon. In this work, DSG is chosen due to its several superior properties[19]. In the other frontier of developing advanced FEM and overcoming the "overly-stiff" drawback of FEM, a family of smoothed finite element methods (S-FEM) was developed by Liu et al. based on the so-called weakened weak formulation using the gradient smoothing technique[20–22]. These novel S-FEM methods have been found and proven to always be softer than the FEM counterpart and offer desirable ways to effectively "soften" the numerical model. The cell-based smoothing finite element method (CS-FEM) was firstly developed, which works well for heavily distorted elements and the general n-sided polygonal elements[20]. Then node-based smoothed finite element method (NS-FEM)[21] was developed for overly-soft behavior so as to produce upper bound solutions (for force driven problems). It is found instable temporally due to the overly-soft feature. Therefore, stabilization techniques are needed when NS-FEM is used to solve dynamic problems[22]. A soft yet temporal stable model, known as the edge-based smoothed finite element (ES-FEM) that exhibits "ultra" accuracy and super convergence properties, was also formulated. In addition, it is found to be the best performer of all the linear models developed so far for structural dynamic problems[23–25]. For the above reasons, we choose ES-FEM together with DSG technique to model the structure part of our structural acoustic problems.

The standard BEM is based on the boundary integral equation (BIE) formulations, which discretizes only the boundary of the problem domain leading to a small set of discretized system equations. In addition, it is ideal for handling problems of infinite domains. Due to these two major features, BEM has been found effective for wave propagation problems such as the acoustics, and particularly attractive for acoustics in infinite exterior domains. BEM has been applied in acoustic area for more than four decades[26–28]. However, due to its computational inefficiency in establishing the discretized system equations that is usually fully-populated and badly conditioned, BEM is limited to solving models with small or medium sizes. Over the past decades, many techniques are applied to improve the overall solution efficiency of BEM. Techniques including H-matrices[29], the wavelet basis[30], the fast Fourier transform[31] and the fast multipole method[32,33] are adopted to accelerate the matrix–vector multiplication. Efficient iterative solvers, such as the generalized minimum residue (GMRES) method[34] and the conjugate gradient squared (CGS) method[35] are also chosen to solve the system of equations of a BEM model. Among all these advances in BEM, the FM-BEM stands out for its outstanding efficiency, and hence is chosen for modeling the acoustic fluid, especially where there is an exterior acoustic media involved.

The FM-BEM method has two key techniques to be implemented. One is the fast multipole method (FMM), which was first introduced by Rokhlin[36] in the mid 1980s. The fundamental principle of the FMM is a multipole expansion of the kernel by which the direct connection between the source point and the collocation point is separated. Another is the use of iterative equation solvers, such as the GMERS[34]. With these two techniques, the FM-BEM[37–42] can reduce the matrix vector multiplication dramatically. In addition, the memory requirement is also reduced. The application of FM-BEM in acoustics was introduced in detail by Nail et al.[40].

This research aims to take advantages of both ES-FEM and FM-BEM techniques to model structural acoustic systems. Through such coupling, we attempt to avoid drawbacks of the "overly-stiff" behavior in the FEM for the vibrating structure, and computational inefficiency in the BEM for the interior acoustic chamber and exterior acoustic media. Considering the huge difference in density between the solid structure and air as the acoustic media, the feedback of the acoustic air onto the structure is neglected in this work. This means that only a "weak coupling" or one way coupling from the solid structure to the air will be taken into consideration. The ES-FEM is applied to approximate the vibrations of the structure, whose normal velocities solution are imposed as boundary conditions for the acoustic domain. The FM-BEM is used to simulate both the frequency responses in interior region and sound field distributions in the exterior region.

The paper is organized as follows: In Sec. 2, we begin with a brief description of basic ES-FEM formulations implemented with DSG method for 2D structure domain. In Sec. 3, Galerkin weak form and discretized system equations for 3D acoustic problems are firstly presented, and then the edge-based gradient smoothing operation for 3D acoustic problems is briefly introduced. In Sec. 4, conventional BEM formulation for 3D acoustic problems is firstly reviewed, and then the multipole expansion theory, which is the fundamental of the FM-BEM, is simply described. In Sec. 5, numerical examples and application are presented to demonstrate the efficiency and validity of the coupled ES-FEM/FM-BEM. Finally, a summary is given in Sec. 6 to conclude this work.

2 ES-FEM FORMULATIONS FOR PLATE STRUCTURE

Consider a vibrating plate subjected to external excitations. The vibrating plate is modeled using 3-nodes triangle plate elements based on the low order Reissner–Mindlin plate theory. The Reissner–Mindlin theory is intended for thick plates in which the normal to the mid-surface remains straight but not necessarily perpendicular to the mid-surface. Due to its simplicity and efficiency, Reissner–Mindlin theory is useful and practical for modeling plates that are not "thin" where the classic plate theory is no longer valid. However, when it is applied to thin plates, these low-order plate elements often suffer from the so-called "shear locking." This is due to that the transverse shear strains cannot vanish under the pure bending condition based on the Reissner–Mindlin theory. In order to eliminate the shear locking, discrete shear gap triangular element (DSG) method[19] has been utilized to overcome the shear locking problem, together with the edge-based smoothed techniques. For easy reference, this technique is termed as ES-FEM-DSG3, where "3" stands for the fact that we use only triangular elements. Because we use only triangular elements, the geometry of the plate can be practically arbitrary.

2.1 ES-FEM-DSG3 Formulations Based on the Reissner–Mindlin Plate

Based on the Reissner–Mindlin plates theory, the unknown vector of three independent field variables at any point in the problem domain of structure can be defined as $\mathbf{u} = \{\theta_x, \theta_y, w\}^T$, where θ_x and θ_y are the rotation angles of the line normal to the undeformed neutral surface in the x–z and y–z planes, respectively, and w is the deflection. The dynamic variation equation for Reissner–Mindlin plate elements without damping can be described as follows[43]:

$$\int_{\Omega_s} \delta\varepsilon_b^T \mathbf{D}_b \varepsilon_b d\Omega + \int_{\Omega_s} \delta\varepsilon_s^T \mathbf{D}_s \varepsilon_s d\Omega + \int_{\Omega_s} \delta\mathbf{u}^T \rho t \omega^2 \mathbf{u} d\Omega - \int_{\Gamma_s} \delta\mathbf{u}^T \tau d\Omega = 0, \quad (1)$$

where the bending stiffness constitutive coefficients $\mathbf{D}_b$, and transverse shear stiffness constitutive coefficients $\mathbf{D}_s$ are defined as:

$$\mathbf{D}_b = \frac{Et^3}{12(1-\nu^2)} \begin{bmatrix} 1 & \nu & 0 \\ \nu & 1 & 0 \\ 0 & 0 & 1-\nu/2 \end{bmatrix},$$
$$\mathbf{D}_s = \kappa t G \begin{bmatrix} 1 & 0 \\ 0 & 1 \end{bmatrix}, \quad (2)$$

in which E represents Young's modulus, ν is the Poisson ratio, G is the shear modulus, and κ is the shear correction factor that is set as 5/6 in this work.

The unknown field variable displacements can be approximated by nodal displacements using shape function:

$$\mathbf{u} = \mathbf{N}_s \mathbf{u}_e = \sum_{i=1}^{n} \mathbf{N}_i(\mathbf{x}) \mathbf{u}_i,$$
$$\delta\mathbf{u} = \mathbf{N}_s \delta\mathbf{u}_e = \sum_{i=1}^{n} \mathbf{N}_i(\mathbf{x}) \delta\mathbf{u}_i, \quad (3)$$

where $\mathrm{N_s}$ is generalized shape functions and $\mathbf{u_e}$ is the vector of generalized nodal displacements for each plate element. N_i and $\mathbf{u}_i = \{\theta_{xi}, \theta_{yi}, w_i\}^T$ are the shape function and nodal variable at node i, respectively. Applying Eqn. (3), the discretized system equations of Eqn. (1) can be written in following matrix form[43]:

$$\mathbf{M}\ddot{\mathbf{u}} + \mathbf{K}\mathbf{u} = \mathbf{F}, \quad (4)$$

where

$$\mathbf{K} = \int_{\Omega} \mathbf{B_b}^T \mathbf{D_b} \mathbf{B_b} d\Omega + \int_{\Omega} \mathbf{B_s}^T \mathbf{D_s} \mathbf{B_s} d\Omega$$
The stiffness matrices (5)

$$\mathbf{M} = \int_{\Omega} \rho \mathbf{N_s}^T \mathrm{diag}\left[\frac{t^3}{12} \quad \frac{t^3}{12} \quad t\right] \mathbf{N_s} d\Omega$$
The mass matrix (6)

$$\mathbf{F} = \int_{\Gamma_s} \mathbf{N_s}^T \tau d\Gamma$$
The vector of nodal forces (7)

where $\mathbf{B_b} = [B_{b1} \quad B_{b2} \quad \cdots \quad B_{bn}]$ is the strain–deflection matrix for bending, $\mathbf{B_s} = [B_{s1} \quad B_{s2} \quad \cdots \quad B_{sn}]$ is the strain–deflection matrix for shearing, t is the thickness of the plate, and τ is the external load on the plate, where:

$$\mathbf{B}_{bi} = \begin{bmatrix} -\frac{\partial N_i}{\partial x} & 0 & 0 \\ 0 & -\frac{\partial N_i}{\partial y} & 0 \\ -\frac{\partial N_i}{\partial y} & -\frac{\partial N_i}{\partial x} & 0 \end{bmatrix},$$
$$\mathbf{B}_{si} = \begin{bmatrix} -N_i & 0 & \frac{\partial N_i}{\partial x} \\ 0 & -N_i & \frac{\partial N_i}{\partial y} \end{bmatrix}. \quad (8)$$

Using the smoothed strain–deflection matrix $\overline{\mathbf{B}}_\mathbf{b}$ and $\overline{\mathbf{B}}_\mathbf{s}$ computed based on the edges of elements to replace $\mathbf{B_b}$ and $\mathbf{B_s}$, the smoothed stiffness can be expressed as:

$$\overline{\mathbf{K}} = \int_{\Omega} \overline{\mathbf{B}}_b^T \mathbf{D}_b \overline{\mathbf{B}}_b d\Omega + \int_{\Omega} \overline{\mathbf{B}}_s^T \mathbf{D}_s \overline{\mathbf{B}}_s d\Omega. \quad (9)$$

The details of computing the smoothing strain–deflection matrices based on the edges can be found in the following sub-section.

Finally, the ES-FEM-DSG3 formulation for structural domain then can be written as:

$$\mathbf{M}\ddot{\mathbf{u}} + \overline{\mathbf{K}}\mathbf{u} = \mathbf{F}. \tag{10}$$

2.2 Edge-Based Smoothing Operation for the Plate Structure

In this section, edge-based smoothed finite element method or ES-FEM for plates is introduced. The plate domain is first discretized using a set of 3-node triangles just as in the standard FEM. Because the Reissner–Mindlin theory uses the derivatives of the deflection to compute the strains, only the stiffness matrix is smoothed in the ES-FEM. The assembling of the stiffness matrix and the integration is based on the smoothing domains which is associated with the edges of the triangles. Using the edges of these triangles, we are able to construct N_s smoothing domains. For edge k, the smoothing domain Ω_k is constructed by connecting the centroids of the neighbor triangles and the end-points of edge k. As shown in Fig. 1, for interior edges, the smoothing domain Ω_k is a quadrangle which is the assembly of the sub-domains of two neighboring elements; while for edges on the plate boundary, the smoothing domain Ω_k is only a single (triangular) sub-domain. The following are the details of the calculation of the smoothed stiffness matrix for the 2D structure problem.

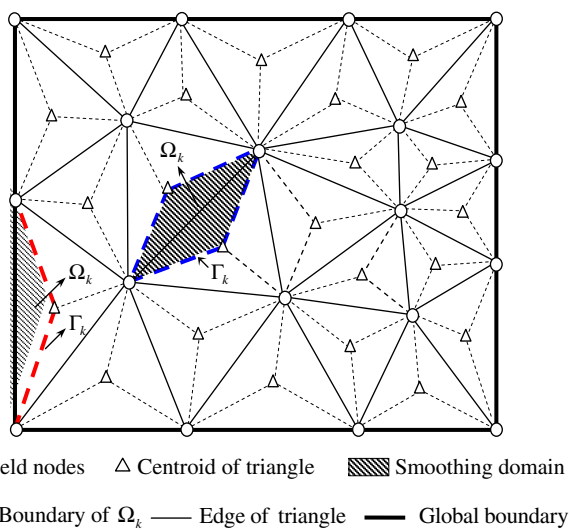

Fig. 1—Triangular mesh for a plate for ES-FEM model and edge-based smoothing domains constructed by connecting the centroids of the neighbor triangles and the two end-points of edge k.

The smoothing operation is firstly applied to the bending (in-plane) strain and the shear (off-plane) stain of the plate over each of the edge-based smoothing domains:

$$\overline{\boldsymbol{\varepsilon}}_b(\mathbf{x}_k) = \frac{1}{A_k}\int_{\Omega_k} \boldsymbol{\varepsilon}_b(\mathbf{x})\, d\Omega,$$
$$\overline{\boldsymbol{\varepsilon}}_s(\mathbf{x}_k) = \frac{1}{A_k}\int_{\Omega_k} \boldsymbol{\varepsilon}_s(\mathbf{x})\, d\Omega, \tag{11}$$

where A_k is the area of the smoothing domain Ω_k, which can be calculated as follows:

$$A_k = \int_{\Omega_k} d\Omega = \frac{1}{3}\sum_{i=1}^{N_k^e} A_e^i \tag{12}$$

in which N_k^e is the number of the sub-domain of edge k (that is either 2 for interior edges or 1 for edges on the plate boundary), and A_e^i is the area of ith sub-domain in a triangle element.

Based on the assumption made in the Reissner–Mindlin plate theory, the bending strain can be expressed as follows[5].

$$\overline{\boldsymbol{\varepsilon}}_b(\mathbf{x}_k) = \sum_{i\in M_k} \overline{\mathbf{B}}_{bi}(\mathbf{x}_k)u_i, \tag{13}$$

where M_k is the total number of vertex of the smoothing domain, which is either 4 for interior edges and 3 for edges on the plate boundary.

When the thickness of plates becomes small, the Reissner–Mindlin plates often suffer the shear locking phenomenon. In order to avoid such a locking, the shear strain is calculated using discrete shear gap triangular element (DSG) method[19]. Combining with the smoothing operation, the smoothed shear strain matrix can be calculated as follows:

$$\overline{\boldsymbol{\varepsilon}}_s(\mathbf{x}_k) = \sum_{i\in M_k} \overline{\mathbf{B}}_{si}(\mathbf{x}_k)u_i, \tag{14}$$

where the smoothed strain matrix $\mathbf{B}_{bi}(x_k)$ and $\mathbf{B}_{si}(x_k)$ in Eqns. (13) and (14) can be calculated by combining with the Eqns. (11) and (12):

$$\overline{\mathbf{B}}_{bi}(\mathbf{x}_k) = \frac{1}{A_k}\sum_{i=1}^{N_k^e}\frac{1}{3}A_e^i\mathbf{B}_{bi}(\mathbf{x}_k),$$
$$\overline{\mathbf{B}}_{si}(\mathbf{x}_k) = \frac{1}{A_k}\sum_{i=1}^{N_k^e}\frac{1}{3}A_e^i\mathbf{B}_{si}(\mathbf{x}_k). \tag{15}$$

More details about $\mathbf{B}_{bi}(x_k)$ and $\mathbf{B}_{si}(x_k)$ based on Reissner–Mindlin plate theory and the discrete shear

gap triangular element (DSG) method can be found in Ref. 19.

Using the smoothed strain matrix $\overline{\mathbf{B}}_s$ and $\overline{\mathbf{B}}_b$, the smoothed strain stiffness matrix $\overline{\mathbf{K}}_b^{(k)}$ and smoothed shear stiffness matrix $\overline{\mathbf{K}}_s^{(k)}$ for the edge-based smoothed domain k can be evaluated as:

$$\begin{aligned}\overline{\mathbf{K}}_b^{(k)} &= \int_{\Omega_k} \overline{\mathbf{B}}_b{}^T \mathbf{D}_b \ \overline{\mathbf{B}}_b d\Omega \\ &= \sum_{k=1}^{N_s} A_k \ \overline{\mathbf{B}}_b{}^T \mathbf{D}_b \ \overline{\mathbf{B}}_b, \\ \overline{\mathbf{K}}_s^{(k)} &= \int_{\Omega_k} \overline{\mathbf{B}}_s{}^T \mathbf{D}_s \ \overline{\mathbf{B}}_s d\Omega \\ &= \sum_{k=1}^{N_s} A_k \ \overline{\mathbf{B}}_s{}^T \mathbf{D}_s \ \overline{\mathbf{B}}_s. \end{aligned} \tag{16}$$

The global smoothed bending stiffness $\overline{\mathbf{K}}_b$ and global smoothed shear stiffness $\overline{\mathbf{K}}_s$ based on the edges can be assembled just as the same procedure as in the standard FEM. Then the global smoothed stiffness can be evaluated as:

$$\overline{\mathbf{K}} = \overline{\mathbf{K}}_b + \overline{\mathbf{K}}_s. \tag{17}$$

If the smoothing operation based on the edges is only applied to bending stiffness $\mathbf{K}_\mathrm{b}$ or shear stiffness $\mathbf{K}_\mathrm{s}$, and the other one remains un-smoothed, we can obtain two variant forms of ES-FEM, where the global stiffness are computed using:

$$\overline{\mathbf{K}}_{(B)} = \overline{\mathbf{K}}_b + \mathbf{K}_\mathbf{s}, \tag{18}$$

where $\overline{\mathbf{K}}_{(B)}$ is global smoothed stiffness with only the bending stain smoothed. It is denoted as ES(B)-FEM. Alternatively,

$$\overline{\mathbf{K}}_{(S)} = \mathbf{K}_b + \overline{\mathbf{K}}_s, \tag{19}$$

where $\overline{\mathbf{K}}_{(S)}$ is global smoothed stiffness with only the shear stain smoothed. It is denoted as ES(S)-FEM.

3 ES-FEM FORMULATIONS FOR 3D ACOUSTIC PROBLEMS

Note that the ES-FEM is applicable also to acoustic problems, and this section briefs the process.

3.1 GS-Galerkin Weak Form and Discretized System Equations

In the acoustic domain, we firstly define an enclosed cavity Ω_f with Neumann boundary Γ_N, assuming that the fluid is homogeneous, inviscid, compressible and only undergoes small translational movement. Letting p denote the acoustic pressure and k denote the wave number, the governing equation for the sound pressure can be expressed as:

$$\Delta p + k^2 p = 0, \text{ in } \Omega_f, \tag{20}$$

where Δ is the Laplace operator, the wave number can be written as $k = \omega/c$, ω is the angular frequency of the pressure oscillation, and c is the speed of sound traveling in the acoustic fluid.

The Neumann boundary of the acoustic domain can be defined as the following:

$$\nabla p \cdot n = -j\rho\omega v_n, \text{ on } \Gamma_N \tag{21}$$

where $j = \sqrt{-1}$, ρ is the density of medium. v_n denotes normal velocity on the boundary. The field variable pressure can be approximated using a shape function, defined as:

$$p = \sum_{i=1}^{m} N_i p_i = \mathbf{N}\mathbf{p}, \tag{22}$$

where P_i denotes the unknown nodal pressure and N_i are shape functions in node i. $\mathbf{N}$ is the generated shape function and $\mathbf{P}$ is the vector of generated pressure for each tetrahedron element.

Applying the Eqn. (22), using shape function as the weight function, the standard Galerkin weak form for acoustic problem without acoustical damping can be written as[25]:

$$\begin{aligned} &-\int_\Omega \nabla\mathbf{N}\cdot\nabla\mathbf{N}\mathbf{P}\, d\Omega + k^2 \int_\Omega \mathbf{N}\cdot\mathbf{N}\mathbf{P} d\Omega \\ &\quad - j\rho\omega \int_{\Gamma_N} \mathbf{N}\cdot v_n d\Gamma \\ &\quad = 0. \end{aligned} \tag{23}$$

Using the smoothed item $\overline{\nabla\mathbf{N}}$ based on the edges of elements to replace the gradient component $\nabla\mathbf{N}$, the generalized smoothed Garlerkin (GS-Galerkin) weak formulation for acoustic problem can be written as:

$$\begin{aligned} &-\int_\Omega \overline{\nabla\mathbf{N}}\cdot\ \overline{\nabla\mathbf{N}}\mathbf{P} d\Omega + k^2 \int_\Omega \mathbf{N}\cdot\mathbf{N}\mathbf{P} d\Omega \\ &\quad - j\rho\omega \int_{\Gamma_N} \mathbf{N}\cdot v_n d\Gamma \\ &\quad = 0. \end{aligned} \tag{24}$$

Finally, the discretized system equations in Eqn. (24) can be written in following matrix form:

$$\mathbf{K} = \int_\Omega \left(\overline{\nabla\mathbf{N}}\right)^T \ \overline{\nabla\mathbf{N}} d\Omega. \tag{25}$$

where:

$$\mathbf{K} = \int_{\Omega} \left(\overline{\nabla \mathbf{N}}\right)^{T} \overline{\nabla \mathbf{N}} d\Omega$$

The smoothed acoustical stiffness matrix (26)

$$\mathbf{M} = \int_{\Omega} \mathbf{N}^{T} \mathbf{N} d\Omega$$

The acoustical mass matrix (27)

$$\mathbf{F} = \int_{\Gamma_N} \mathbf{N}^{T} v_n d\Gamma$$

The vector of nodal acoustic forces (28)

$$\{\mathbf{P}\}^{T} = \{p_1, p_2 \cdots, p_n\}$$

Nodal acoustic pressure in the domain (29)

3.2 Edge-Based Gradient Smoothing Operation for 3D Acoustic Domain

In this section, the formulation of ES-FEM for 3D acoustic fluid is presented. The acoustic domain is divided exactly as that of standard FEM using four node tetrahedral elements. The edge-based gradient smoothing domains, which are also serving as integration domains, are then formed in association with these tetrahedral elements. As shown in Fig. 2, the sub-smoothing domain of edge k in cell i is created by connecting the centroid of cell i to the two end-nodes of the edge k and the related surface triangles.

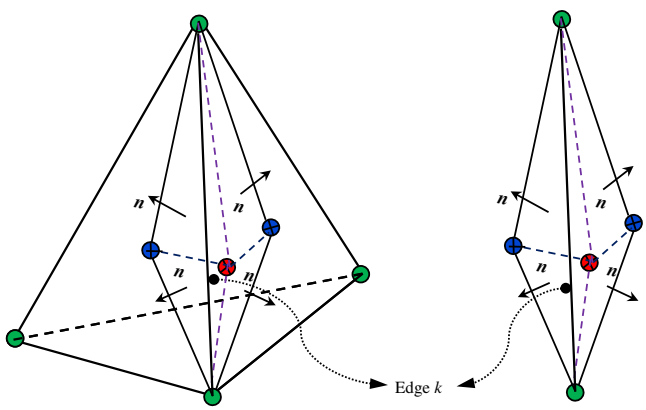

Fig. 2—3D edge-based smoothing domains constructed by connecting the centroid of cell i to end-nodes of the edge k and the related surface triangles.

For acoustic problems, the gradient smoothing operation will be applied over each edge-based smoothing domain on the velocity v. The smoothed velocity, which is deduced by the gradient of acoustic pressure, is denoted as:

$$\overline{v}(\mathbf{x}_k) = \frac{1}{V_k} \int_{\Omega_k} v(\mathbf{x}) d\Omega, \tag{30}$$

where $V_k = \int_{\Omega_k} d\Omega$ denotes the volume of smoothing domain for edge k.

The smoothed velocity can be expressed in terms of acoustic pressure by applying the Green's theorem:

$$\overline{v}(\mathbf{x}_k) = -\frac{1}{j\rho\omega V_k} \int_{\Omega_k} \nabla p d\Omega$$

$$= -\frac{1}{j\rho\omega V_k} \int_{\Gamma_k} p \cdot n d\Gamma. \tag{31}$$

Substituting the field variable (acoustic pressure) interpolation in form of Eqn. (22) into Eqn. (31), the smoothed velocity for edge k can be denoted as the following matrix form:

$$\overline{v}(\mathbf{x}_k) = -\frac{1}{j\rho\omega} \sum_{I \in M_k} \overline{\mathbf{B}}_i(\mathbf{x}_k) p_i, \tag{32}$$

where M_k represents the total number of nodes in the smoothing domain of edge k. $\overline{\mathbf{B}}_\mathbf{i}$ can be defined as:

$$\overline{\mathbf{B}}_i^{T}(\mathbf{x}_k) = \left[\, \overline{b}_{i1} \;\; \overline{b}_{i2} \;\; \overline{b}_{i3} \right] \tag{33}$$

$$\overline{b}_{ip} = \frac{1}{V_k} \int_{\Gamma_k} N_i(\mathbf{x}) n_p(\mathbf{x}) d\Gamma. \tag{34}$$

Finally, the smoothed stiffness matrix shown in Eqn. (25) can be assembled based on the smoothed $\overline{\mathbf{B}}$ as:

$$\overline{\mathbf{K}}^{(k)} = \int_{\Omega_k} \overline{\mathbf{B}}^{T} \; \overline{\mathbf{B}} d\Omega = \sum_{k=1}^{N_s} V_k \; \overline{\mathbf{B}}^{T} \; \overline{\mathbf{B}}. \tag{35}$$

Owning to the compact supports of the FEM shape functions, the assembled smoothed stiffness matrix Eqn. (35) is banded and symmetric. Therefore system equations can be solved efficiently, even though it discretizes the entire domain, as long as the domain is enclosed. However, when it is used for exterior media (that is infinite), some kind of non-reflecting boundary techniques[44] must be used. In such cases, the FM-BEM can be a better choice, because there is no need for artificial non-reflecting boundary.

4 FAST MULTIPOLE BEM FOR ACOUSTIC PROBLEMS

4.1 Conventional BEM Formulations for Acoustic Problems

In this section, we first review the conventional BEM formulation for Helmholtz equations. The fundamental solution or the full-space Green's function for acoustic problems is well-known and can be denoted as follows[45]:

$$G(x,y)=\frac{e^{-jk|x-y|}}{4\pi|x-y|}, \tag{36}$$

where $j=\sqrt{-1}$, k is the wavenumber, and $|x-y|$ is the distance between the collocation point x and the source point y.

Combining the conventional boundary integral equation (CBIE) and the hypersingular boundary integral equation (HBIE), a well-known integral equation, named as CHBIE formulation, for Helmholtz equation in Eqn. (20) without the incident wave can be written as[45]:

$$\begin{aligned}&\left[\int_{\Gamma}\frac{\partial G(x,y)}{\partial n(y)}p(y)d\Gamma(y)+C(x)p(x)\right]\\&+\alpha\int_{\Gamma}\frac{\partial^2 G(x,y)}{\partial n(y)\partial n(x)}p(y)d\Gamma(y)\\&\quad=\int_{\Gamma}G(x,y)q(y)d\Gamma(y)\\&+\alpha\left[\int_{\Gamma}\frac{\partial G(x,y)}{\partial n(x)}q(y)d\Gamma(y)-C(x)q(x)\right]\\&\forall x\in\Gamma.\end{aligned} \tag{37}$$

where q is defined as $q=\frac{\partial p}{\partial n}$. The constant $C(x)$ is set as 1/2 for smooth surface around x, and the coupling constant α is defined as j/k.

Dividing the boundary into N surface elements, the discretized form of the CHBIE formulation can be expressed as[45]:

$$\sum_{j=1}^{N}f_{ij}p_j=\sum_{j=1}^{N}g_{ij}q_j. \tag{38}$$

where:

$$\begin{aligned}f_{ij}p_j&=\int_{\Delta\Gamma_j}\frac{\partial G(x,y)}{\partial n(y)}p_j d\Gamma(y)+\frac{1}{2}\delta_{ij}p_j\\&+\alpha\int_{\Delta\Gamma_j}\frac{\partial^2 G(x,y)}{\partial n(y)\partial n(x)}p_j d\Gamma(y)\end{aligned}$$

$$\begin{aligned}g_{ij}q_j&=\int_{\Delta\Gamma_j}G(x,y)q_j d\Gamma(y)\\&+\alpha\left[\int_{\Delta\Gamma_j}\frac{\partial G(x,y)}{\partial n(x)}q_j d\Gamma(y)-\frac{1}{2}\delta_{ij}q_j\right],\end{aligned} \tag{39}$$

where δ_{ij} is the Kronecker Delta, and $\Delta\Gamma_j$ denotes element j.

The discretized form of the Burton–Miller formulation in Eqn. (38) can be transformed to the following system of equations by moving the known terms to the right-hand side and the unknown terms to the left-hand side.

$$\begin{bmatrix}a_{11}&a_{12}&\cdots&a_{1N}\\a_{21}&a_{22}&\cdots&a_{2N}\\\vdots&\vdots&\ddots&\vdots\\a_{N1}&a_{N2}&\cdots&a_{NN}\end{bmatrix}\begin{Bmatrix}\lambda_1\\\lambda_2\\\vdots\\\lambda_N\end{Bmatrix}=\begin{Bmatrix}b_1\\b_2\\\vdots\\b_N\end{Bmatrix}\text{or}\qquad\mathbf{A\lambda=b} \tag{40}$$

where $\mathbf{A}$, $\boldsymbol{\lambda}$ and $\mathbf{b}$ are the system matrix, unknown vector and known vector, respectively.

4.2 The Fast Multipole Method Implemented in BEM

There are two main techniques applied to improve the efficiency of the conventional BEM. Firstly, the fast multipole method (FMM) is employed to speed up the matrix–vector multiplication in $\mathbf{A\lambda}$, then an efficient iterative solver, such as the generalized minimum residue method (GMRES), will be applied to solve the system of equations given by Eqn. (40). With FMM, the fast multipole boundary element method can be constructed. The fundamental principle of the FMM is a multipole expansion of the kernel in which the direct connection between the source point and the collocation point is separated. The details of the derivations of the FM-BEM formulations can be found in Refs. 40 and 45. With the fast multipole BEM, acoustic BEM models with DOFs up to several millions have been solved on laptop PCs with a RAM size of only 8 GB.

5 NUMERICAL EXAMPLES

In this section, two numerical applications of 3D cases are presented, in order to verify the effectiveness of the proposed combination of ES-FEM and FM-BEM formulations. Because of the huge difference existing in terms of mass density of the structure and

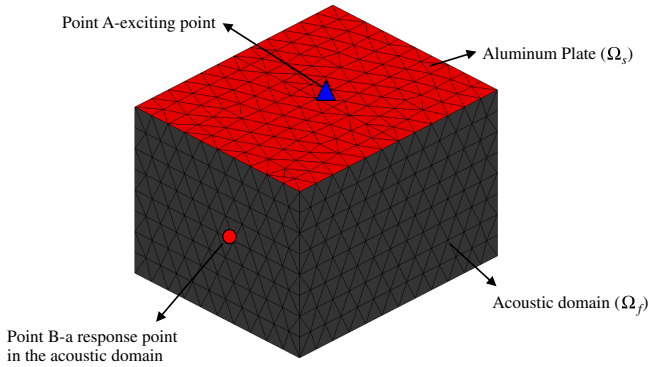

Fig. 3—A flexible aluminum plate backed by a box of air.

air, acoustic modes are not coincident with the structural modes; it is thus practical to neglect direct interactions between the structure and air[46], meaning that the structure dynamics is assumed not to be influenced by the fluid. For comparison, the results obtained from the FEM with extremely fine mesh are also provided as the reference results. The purpose of the first example of a simple elastic plate backed by a closed acoustic cavity is to show the advantages of ES-FEM and FM-BEM. The second example is an application of the present combined methods to a practical problem in vehicle engineering.

5.1 Box with Flexible Plate on Top

In this subsection, a weak coupling model of a flexible plate and air cavity is established. The model is shown in Fig. 3. The weakly coupled model is a combination of the flexible plate on the top and a closed acoustic cavity attached. The elastic plate is made of aluminum (ρ = 2700 kg/m^3, ν = 0.3 and E = 71 Gpa). The acoustic cavity is full of air (ρ = 1.21 kg/m^3 and c = 343 m/s). The plate, which has a dimension of 0.50 m × 0.60 m and a thickness of t = 0.003 m, is simply supported on all the four edges. The closed acoustic cavity has a dimension of 0.50 m × 0.60 m × 0.40 m. The remaining walls (except the coupled wall) of cavity are assumed to be rigid with the surface velocity fixed at v = 0.

The top elastic plate is divided with Reissner–Mindlin triangle plate elements. An evenly distributed time harmonic load equal to 100 N is applied at the center of plate (point A in Fig. 3). First, the forced frequency responses are computed at the center of the plate using different methods including FEM, ES-FEM, ES(B)-FEM and ES(S)-FEM with same model (155 nodes, 264 elements). The frequency ranges from 1 to 1000 Hz. The reference result is provided using FEM with much smaller elements (1265 nodes, 2390 elements).

As shown in Fig. 4, in the low frequency domain (0 to 200 Hz), results obtained from FEM and ES-FEM show excellent agreements with the reference result, demonstrating that both FEM and ES-FEM can provide accuracy results in low frequencies. As the frequency increases, the deviation between FEM result and the reference result becomes larger, suggesting that the accuracy of the FEM result decreases with the increase of the frequency. We also note that the eigen-frequencies in FEM result (peaks in response curve) become higher and higher compared to the reference result. This deviation mainly results from the inherent drawback of "over-stiffness" in FEM based on the standard weak formulation. The ES-FEM provides much more accurate result in higher frequency range, compared to the FEM model using the same mesh. From Fig. 5, we can see that ES(B)-FEM can also produce results similar to that of ES-FEM. The softening effect of ES(B)-FEM is almost equal to that of ES-FEM. In addition, as showed in Fig. 6, the response curves obtained from

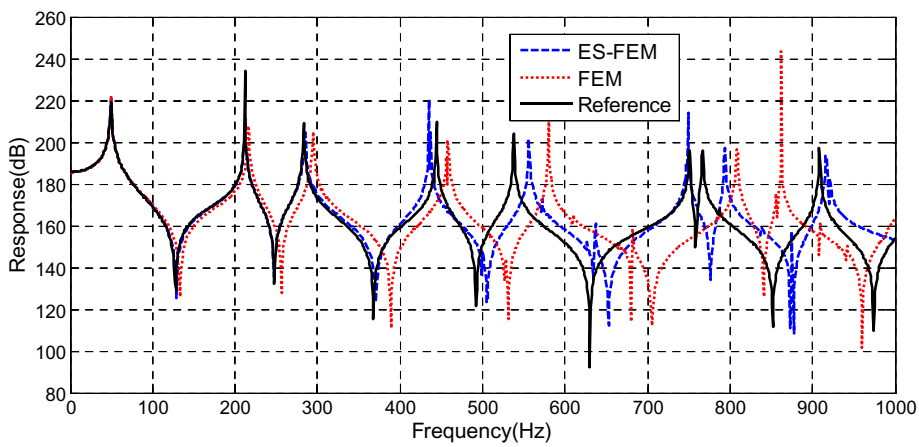

Fig. 4—Frequency responses computed at point A using ES-FEM and FEM for the plate alone.

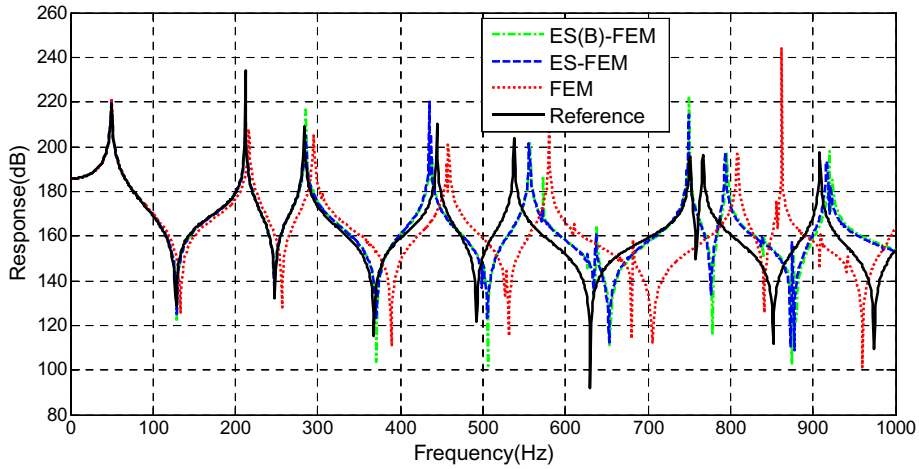

Fig. 5—Frequency responses computed at point A using ES(B)-FEM, ES-FEM and FEM for the plate alone.

ES(S)-FEM have little difference from that of FEM (using the same mesh), which means that the softening effect by the edge-based smoothing on the off-plane shear strain is minimum and can be neglected. Therefore, it can be concluded that the total softening effects of ES-FEM are mainly due to smoothing the in-plane bending strain.

The sound pressure level (SPL) responses at point B in acoustic domain (Fig. 3) are also computed using various combination of methods, and the results are plotted in Fig. 7. The normal velocity of the flexible plate, which provides the boundary condition of acoustic domain, is approximated using ES-FEM and FEM. The 3D acoustic domain is divided using tetrahedron elements (1045 nodes, 6335 elements) for FEM and ES-FEM. If FM-BEM is chosen, only the surface of the 3D acoustic domain is discretized with triangle elements, and hence the number of elements is much smaller (634 nodes, 1264 elements). The computation is performed for frequencies ranging from 1 to 700 Hz. For comparison, the numerical result obtained by the coupled FEM/FEM with a very fine mesh (15,864 nodes and 82,858 elements) is presented as the reference.

As shown in Fig. 7, the coupled FEM/FEM gives the least accurate results compared to all the other models. The over-stiffness phenomenon of FEM in 3D acoustic problems can also be observed, and it becomes much more pronounced with the increase of the frequency. The stiffness matrix in coupled ES-FEM/ES-FEM is softer, and hence the results in high frequency range show better agreements with reference results. The coupled ES-FEM/FM-BEM model has almost the same level accuracy as the coupled ES-FEM/ES-FEM model. It is found that the FM-BEM can offer accurate results for interior acoustic problems.

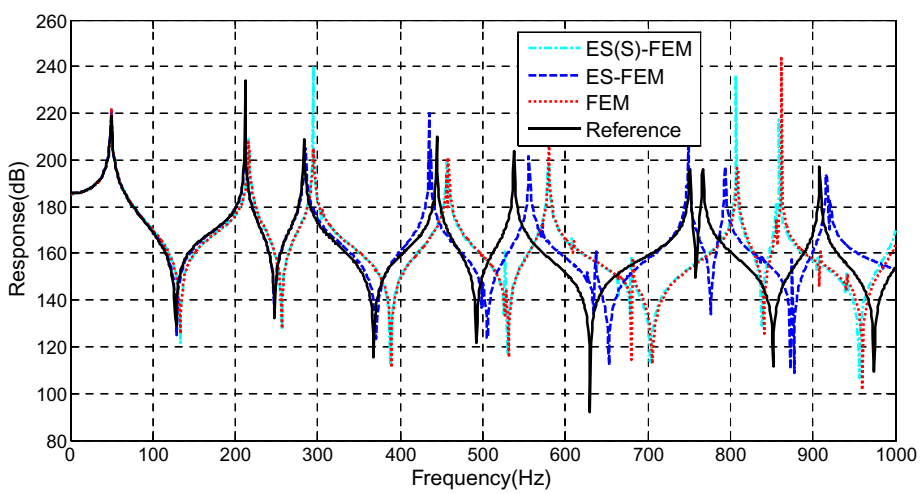

Fig. 6—Frequency response analysis in point A using ES(S)-FEM, ES-FEM and FEM for the plate alone.

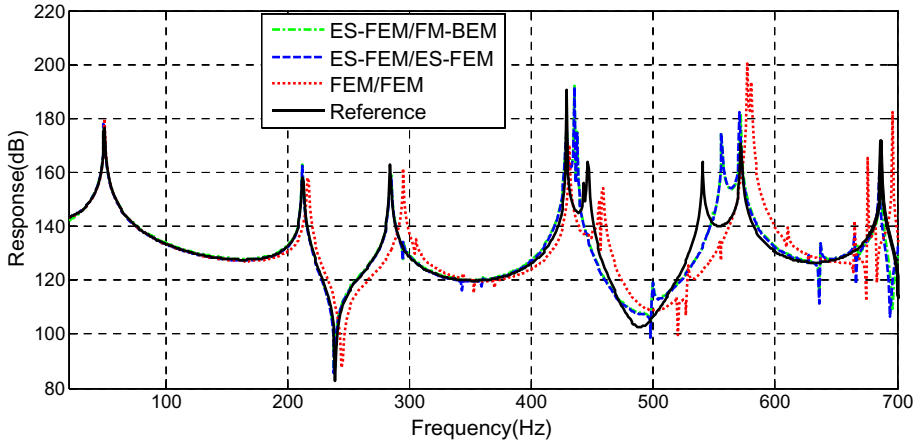

Fig. 7—The sound pressure level (SPL) responses computed at point B using ES-FEM/FM-BEM, ES-FEM/ES-FEM and FEM/FEM.

5.2 Automobile Passenger Compartment with a Flexible Roof

In this example, the application of the present combined method (ES-FEM and FM-BEM) to a practical problem of vehicle engineering is examined. The vehicle body is made of panels, and is usually welded with numerous thin steel plates, among which, the automobile coping is one of the largest structures in the vehicle. The roof can be easily excited, and undergoes low amplitude vibration, generating noises, which contributes strongly to both the interior sound pressure level (SPL) in the automobile passenger compartment and the exterior noise pressure distribution.

In this study, a weak coupling model between the flexible roof and the passenger compartment is established as shown in Fig. 8. The boundary edges of the roof is totally fixed with $w = 0$, $\theta_x = 0$ and $\theta_y = 0$. It is discretized using 422 Reissner–Mindlin triangle plate elements with 241 nodes. The elastic plate is made of steel (ρ = 7900 kg/m3, v = 0.3 and E = 210 GPa), with a thickness of 0.001 m. The automobile passenger compartment is divided using 139,945 tetrahedron elements with 26,498 nodes for the FEM and ES-FEM. When the acoustic domain is calculated using FM-BEM, only the surface of the 3D acoustic domain is meshed with constant triangle elements that are much less in numbers (11,550 elements and 5777 nodes). An evenly distributed time harmonic load (100 N) is applied in the middle of the coping (exciting point in Fig. 8). Both the interior the sound pressure level (SPL) and the exterior of sound pressure distribution are computed and examined.

The sound pressure level (SPL) responses calculated at driver's ear point obtained using the coupled ES-FEM/FM-BEM and coupled ES-FEM/ES-FEM are plotted in Fig. 9. The results are compared against the reference result that is calculated using coupled FEM/FEM with 630,441 elements and 114,174 nodes.

As shown in Fig. 9, the results for this complicated example reinforces the finding from the previous simple example. The response results from the ES-FEM/FM-BEM agree well with that from ES-FEM/ES-FEM. Both results are much more accurate than the FEM/FEM results using the same mesh. In the low frequency range (0 to 40 Hz), all the coupled methods can produce very accurate solutions, which is in a good agreement with the reference result. As the frequency increases, the result obtained from the coupled FEM/FEM becomes inaccurate. Both ES-FEM/FM-BEM and ES-FEM/ES-FEM results have similar level of accuracy, much more accurate than the FEM counterpart, and the eigen-frequencies (peak in response curve) are much closer to that of the reference result.

In order to examine the performance of the ES-FEM/FM-BEM comparing with the conventional ES-FEM/

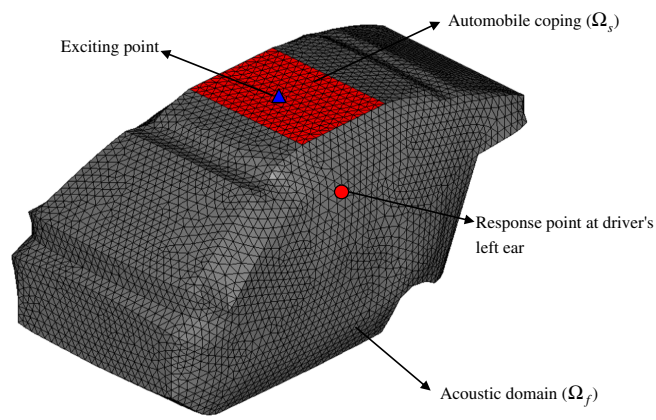

Fig. 8—A weak coupling model combined by the flexible coping and the passenger compartment.

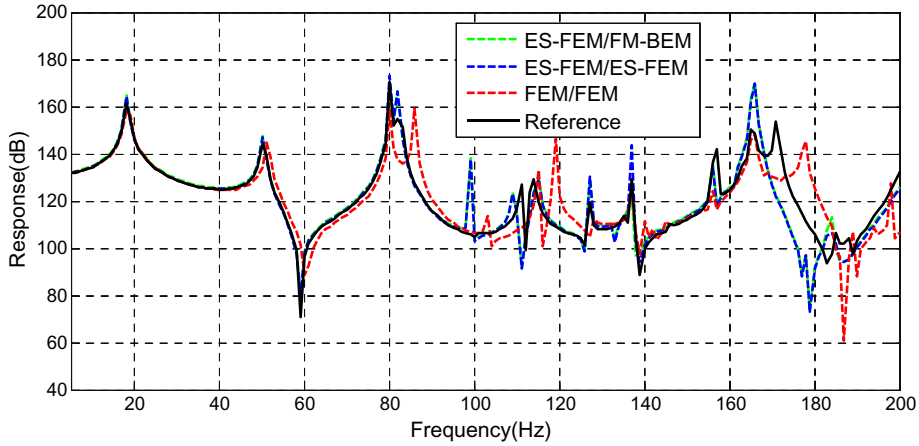

Fig. 9—The sound pressure level (SPL) responses at vehicle driver's ear point obtained using ES-FEM/ES-FEM, ES-FEM/FM-BEM and FEM/FEM.

BEM, the forced frequency response at driver's ear point are computed and plotted in Fig. 10. It is observed that the results obtained from ES-FEM/FM-BEM coincide with the one from ES-FEM/BEM. This indicates that the FMM operation does not lead to any loss of accuracy if the FMM parameters are chosen reasonably. However, the computational efficiency is improved significantly via the FMM operations. The efficiency of ES-FEM/FM-BEM is further evident in the following numerical example.

Solving sound radiation problems is one of the most important and useful application of the boundary integral methods. In this subsection, we further explore the boundary integral approaches using a larger scale problem. The radiation of acoustic waves from vibrating portions of the vehicle body is studied. The vehicle body model, which is used in the previous case, has an overall dimensions of 2.7 m $\times$ 1.4 m $\times$ 1.3 m in the x, y and z direction, respectively, and is meshed with 11,550 constant triangular elements (Fig. 8). For data collection for the velocity potential distribution, a total of 1170 field points are placed on a semi-cylindrical surface with radius of 2.5 m, shown in Fig. 11. The harmonic vibrations of the roof along the z direction are computed by ES-FEM-DSG3, subjected to a harmonic load of 100 N with a frequency of 82.13 Hz, at the center of the coping (exciting point in Fig. 8). The sound pressure distribution on the surface of the semi-column cylinder is computed using the FM-BEM and BEM and shown in Fig. 12. It is found that sound pressure level (SPL) distribution obtained using the ES-FEM/FM-BEM and ES-FEM/BEM is almost the same, which demonstrates that FM-BEM can solve the radiation problem as the BEM without the loss of accuracy. To examine the efficiency of various combination of models, the vehicle body is discretized using different size elements. The CPU time used by the ES-FEM/FM-BEM and the ES-FEM/BEM codes is recorded, and the comparison is shown in Fig. 13. It is clearly shown that the ES-FEM/FM-BEM is much less time-consuming than ES-FEM/BEM in solving all different

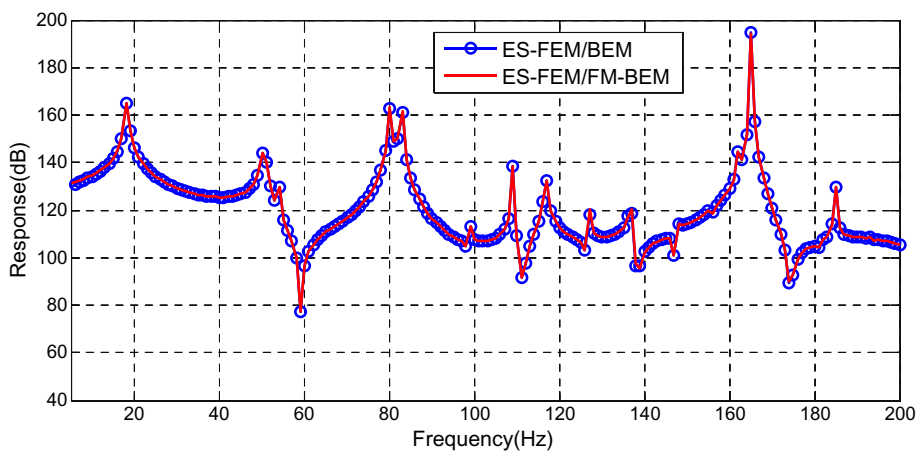

Fig. 10—The sound pressure level (SPL) responses at vehicle driver's ear point obtained using ES-FEM/BEM and ES-FEM/FM-BEM.

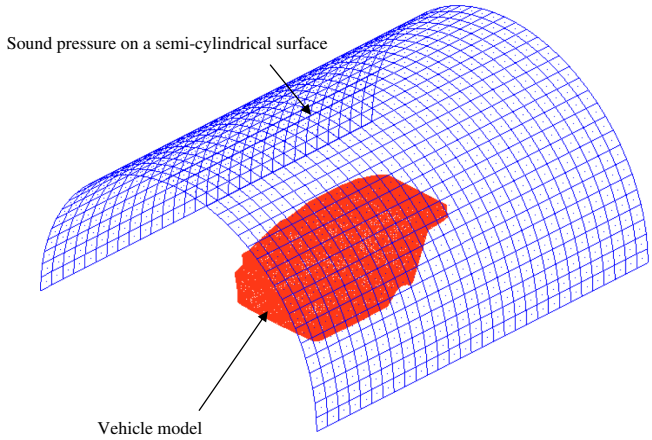

Fig. 11—Semi-cylindrical surface for examining the sound pressure excited by a vibrating coping of vehicle.

sizes of models (DOFs from 4000 to 12,000). The CPU time for the ES-FEM/FM-BEM code scales almost linearly with the increase of the DOFs. The conventional BEM, however, scales about as a cubic function with

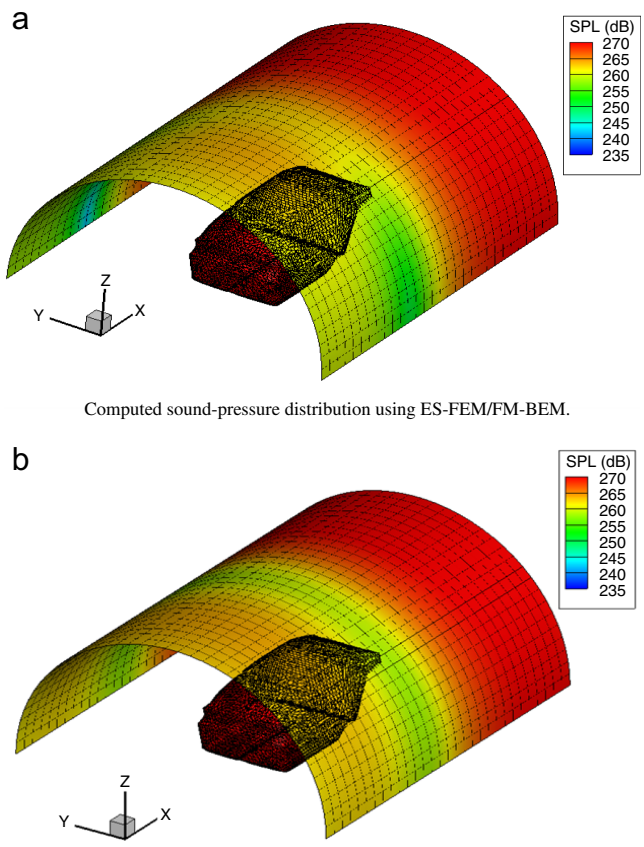

Fig. 12—Computed sound-pressure distribution on a semi-cylindrical surface for the vehicle body model (at 82.13 Hz) using different combined methods.

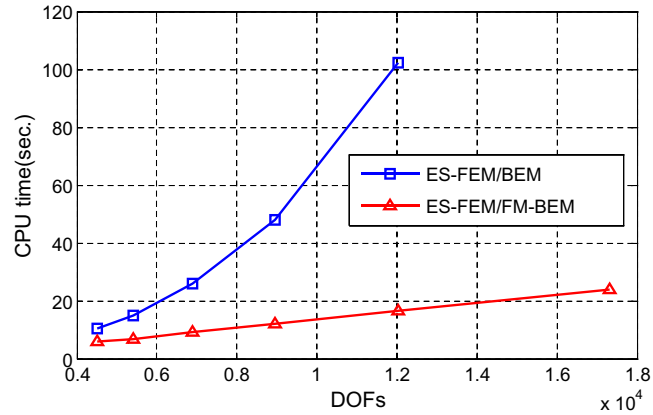

Fig. 13—CPU time used by the ES-FEM/FM-BEM code compared with that of the ES-FEM/BEM code.

the DOFs, and it can only solve models with up to 17,300 DOFs on the same PC.

6 CONCLUSIONS AND DISCUSSIONS

In this paper, a coupled ES-FEM/FM-BEM method is proposed for analyzing structural acoustic problems. Our combined approach takes the best advantages of both ES-FEM and FM-BEM, and the inherent drawbacks of the "overly-stiff" in FEM and computational inefficiency in BEM are overcome. Numerical examples of structural acoustic problems have demonstrated the following features of the present method:

1. For the Reissner–Mindlin plates, the total softening effect of ES-FEM is mainly resulted by smoothing of the in-plane bending strains, while smoothing the shear strain has little effects.
2. The coupled ES-FEM/FM-BEM can produce much more accurate results than that of the FEM/FEM in middle frequency range for interior acoustic problems.
3. The coupled ES-FEM/FM-BEM produces almost the same level of accuracy as the coupled ES-FEM/ES-FEM, which means that the FMM operation in ES-FEM/FM-BEM does not lead to significant loss of accuracy.
4. Owning to the FMM technique and the iterative equation solver (GMERS) applied in FM-BEM, coupled ES-FEM/FM-BEM is much more efficient than ES-FEM/BEM for exterior noise radiation problems, without losing accuracy. It is found that ES-FEM/FM-BEM can be several times faster than ES-FEM/BEM, which is especially crucial for large-scale numerical acoustic problems.

7 ACKNOWLEDGMENTS

The authors wish to thank the support NFSC (61232014) and also the Chinafunded Postgraduates' Studying Aboard Program for Building Top University and the National Natural Science Foundation of China. This work is partially supported by University of Cincinnati. The work by the 2nd author is partially supported by the United States NSF Grant under the award no. 1214188, and partially by the United States ARO contract no. W911NF-12-1-0147.

8 REFERENCES

1. G.C. Everstine, "Finite element formulations of structural acoustics problem", *Computers & Structures*, **65**(3), 307–321, (1997).
2. D. Soares Jr., "Acoustic modeling by BEM–FEM coupling procedures taking into account explicit and implicit multi-domain decomposition techniques", *International Journal for Numerical Methods in Engineering*, **78**, 1076–1093, (2009).
3. M. Fischer and L. Gaul, "Fast BEM-FEM mortar coupling for acoustic-structure interaction", *International Journal for Numerical Methods in Engineering*, **62**(12), 1677–1690, (2005).
4. Z.O. Cecil and R.L. Taylor, *The Finite Element Method: Solid Mechanics*, Vol. 2. Butterworth-Heinemann, (2000).
5. N. Reddy, *Theory and Analysis of Elastic Plates and Shells*. CRC Press: Taylor and Francis Group, New York, (2006).
6. F. Gruttmann and W. Wagner, "A stabilized one-point integrated quadrilateral Reissner–Mindlin plate element", *International Journal for Numerical Methods in Engineering*, **61**, 2273–2295, (2004).
7. J. Mackerle, "Finite element linear and nonlinear, static and dynamic analysis of structural elements: a bibliography", *Engineering Computations*, **19**(5), 520–594, (2002).
8. O.C. Zienkiewicz and R.L. Taylor, *The Finite Element Method*, Fifth Ed., Butterworth-Heinemann, Oxford, (2000).
9. O.C. Zienkiewicz, R.L. Taylor and J.M. Too, "Reduced integration techniques in general of plates and shells", *International Journal for Numerical Methods in Engineering*, **3**, 275–290, (1971).
10. S. Cen, Y.Q. Long and Z.H. Yao, "A new hybrid-enhanced displacement-based element for the analysis of laminated composite plates", *Computers and Structures*, **80**(9–10), 819–833, (2002).
11. S. Cen, A.K. Soh, Y.Q. Long and Z.H. Yao, "A new 4-node quadrilateral FE model with variable electrical degrees of freedom for the analysis of piezoelectric laminated composite plates", *Composite Structures*, **58**(4), 583–599, (2002).
12. P.G. Bergan and X. Wang, "Quadrilateral plate bending elements with shear deformations", *Computers and Structures*, **19**(1–2), 25–34, (1984).
13. S.W. Lee and T.H.H. Pian, "Finite elements based upon Mindlin plate theory with particular reference to the four-node isoparametric element", *AIAA Journal*, **16**, 29–34, (1978).
14. S.W. Lee and C. Wong, "Mixed formulation finite elements for Mindlin theory plate bending", *International Journal for Numerical Methods in Engineering*, **18**, 1297–1311, (1982).
15. J.M.A. César de Sá, R.M. Natal Jorge, R.A. Fontes Valente and P.M.A. Areias, "Development of shear locking-free shell elements using an enhanced assumed strain formulation", *Int. J. Numer. Methods Engrg.*, **53**, 1721–1750, (2002).
16. R.P.R. Cardoso, J.W. Yoon, M. Mahardika, S. Choudhry, R.J. Alves de Sousa and R.A. Fontes Valente, "Enhanced assumed strain (EAS) and assumed natural strain (ANS) methods for one-point quadrature solid-shell elements", *Int. J. Numer. Methods Engrg*, 156–187, (2008).
17. J.L. Batoz and I. Katili, "On a simple triangular Reissner/Mindlin plate element based on incompatible modes and discrete constraints", *Int. J. Numer. Methods Engrg.*, 1603–1632, (1992).
18. O.C. Zienkiewicz, R.L. Taylor, P. Papadopoulos and E. Onate, "Plate bending elements with discrete constraints: new triangular elements", *Comput. Struct.*, 505–522, (1990).
19. K.U. Bletzinger, M. Bischoff and E. Ramm, "A unified approach for shear-locking-free triangular and rectangular shell finite elements", *Comput Struct.*, **75**, 321–34, (2000).
20. G.R. Liu, T.T. Nguyen, K.Y. Dai and K.Y. Lam, "Theoretical aspects of the smoothed finite element method (SFEM)", *International Journal for Numerical Methods in Engineering*, **71**, 902–30, (2007).
21. G.R. Liu, T.T. Nguyen, X.H. Nguyen and K.Y. Lam, "A node-based smoothed finite element method for upper bound solution to solid problems (NS-FEM)", *Comput Struct.*, **87**, 14–26, (2009a).
22. Z.Q. Zhan and G.R Liu, "Temporal stabilization of the node-based smoothed finite element method and solution bound of linear elastostatics and vibration problems", *Computational Mechanics*, **46**, 229–246, (2010).
23. Z.C. He, G.R. Liu, Z.H. Zhong, G.Y. Zhang and A.G. Cheng, "Coupled analysis of 3D structural–acoustic problems using the edge-based smoothed finite element method/finite element method", *Finite Elements in Analysis and Design*, **46**, 1114–1121, (2010).
24. G.R. Liu, T.T. Nguyen and K.Y. Lam, "An edge-based smoothed finite element method (ES-FEM) for static and dynamic problems of solid mechanics", *J. Sound Vibr.*, **320**, 1100–1130, (2009).
25. Z.C. He, G.R. Liu, Z.H. Zhong, S.C. Wu, G.Y. Zhang and A.G. Cheng, "An edge-based smoothed finite element method (ES-FEM) for analyzing three-dimensional acoustic problems", *Computer Methods in Applied Mechanics and Engineering*, **199**(1–4), 20–33, (2009).
26. H.A. Schenck, "Improved integral formulation for acoustic radiation problems", *J. Acoust. Soc. Am.*, **44**(1), 41–58, (1968).
27. A.J. Burton and G.F. Miller, "The application of the integral equation methods to the numerical solution of some exterior boundary-value problems", *Proceedings of the Royal Society of London, Series A, Mathematical Physical & Engineering Sciences*, **323**(1553):201–210, (1971).
28. O. Estorff, *Boundary Elements in Acoustics: Advances and Applications*, WIT Press, Southampton, (2000).
29. W. Hackbusch, "A sparse matrix arithmetic based on H-matrices. Part I. Introduction to H-matrices", *Computing*, **62**(2), 89–108, (1999).
30. G. Beylkin, A. Coifman and V. Rokhlin, "Fast wavelet transforms and numerical algorithms I", *Communications on Pure and Applied Mathematics*, 141–183, (1991).
31. G. Golub and C.V. Loan, *Matrix Computations*, 3rd Ed., The Johns Hopkins University Press, Baltimore, (1996).
32. L. Greengard and V. Rokhlin, "A fast algorithm for particle simulations", *Journal of Computational Physics*, **73**, 325–348, (1987).
33. V. Rokhlin., "A fast algorithm for the discrete Laplace transformation", *Journal of Complex*, **4**(1):12–32, (1988).
34. Y. Saad and M.H. Schultz, "GMRES: a generalized minimal residual algorithm for solving nonsymmetric linear systems", *SIAM Journal on Scientific and Statistical Computing*, **7**, 856–869, (1986).
35. P. Sonneveld, "CGS, A fast Lanczos-type solver for nonsymmetric linear systems. SIAM", *Journal on Scientific and Statistical Computing*, **10**, 36–52, (1986).
36. V. Rokhlin, "Rapid solution of integral equations of classical potential theory", *Journal of Computational Physics*, **60**(2), 187–207, (1985).

37. S. Amini and A.T.J. Profit, “Analysis of a diagonal form of the fast multipole algorithm for scattering theory”, *BIT Numerical Mathematics*, 585–602, (1999).
38. Tetsuya Sakuma and Yosuke Yasuda, “Fast multipole boundary element method for large-scale steady-state sound field analysis. Part I: setup and validation”, *Acta Acustica united with Acustica*, **88**(4), 513–525, (2002).
39. S. Schneider, “Application of fast methods for acoustic scattering and radiation problems”, *Journal of Computational Acoustics*, **11**(3), 387–401, (2003).
40. A. Nail, D. Gumerov and D. Ramani, *Fast Multipole Methods for the Helmholtz Equation in Three Dimensions*, Elsevier Science, (2005).
41. Z.S. Chen, H. Waubke and W. Kreuzer. “A formulation of the fast multipole boundary element method (FMBEM) for acoustic radiation and scattering from three-dimensional structures”, *Journal of Computational Acoustics*, 303–320, (2008).
42. H.J. Wu, Y.J. Liu and W.K. Jiang, “A fast multipole boundary element method for 3D multi-domain acoustic scattering problems based on the Burton–Miller formulation”, *Engineering Analysis with Boundary Elements*, **36**(5), 779–788, (2012).
43. G.R. Liu, *Meshfree Methods: Moving beyond the Finite Element Method*, 2nd Ed, CRC Press, (2009).
44. G.R. Liu and J.D. Achenbach, “A strip element method for stress-analysis of anisotropic linearly elastic solids”, *Journal of Applied Mechanics Transactions of the ASME*, **61**(2), 270–277, (1994).
45. Y.J. Li, *Fast Multipole Boundary Element Method — Theory and Applications in Engineering*. Cambridge University Press, (2009).
46. R. Citarella, L. Federico and A. Cicatiello, “Modal acoustic transfer vector approach in a FEM–BEM vibro-acoustic analysis”, *Engineering Analysis with Boundary Elements*, **31**, 248–258, (2007).